Determination of the bulk melting temperature of nickel using Monte Carlo simulations: Inaccuracy of extrapolation from cluster melting temperatures

Citation: Los, J. H., and R. J. M. Pellenq. "Determination of the bulk melting temperature of nickel using Monte Carlo simulations: Inaccuracy of extrapolation from cluster melting temperatures." Physical Review B 81.6 (2010): 064112. © 2010 The American Physical Society.

As Published: http://dx.doi.org/10.1103/PhysRevB.81.064112

Publisher: American Physical Society

Persistent URL: http://hdl.handle.net/1721.1/57442

Version: Final published version: final published article, as it appeared in a journal, conference proceedings, or other formally published context

Determination of the bulk melting temperature of nickel using Monte Carlo simulations: Inaccuracy of extrapolation from cluster melting temperatures

J. H. Los[1] and R. J. M. Pellenq[1,2]

[1]*Département Théorie et Simulation Numérique, Centre Interdisciplinaire des Nanosciences de Marseille (CINaM), CNRS-UPR 3118, Campus de Luminy, 13288 Marseille, France*

[2]*Department of Civil and Environmental Engineering, MIT, 77 Massachusetts Avenue, Cambridge, Massachusetts 02139, USA*

(Received 14 October 2009; revised manuscript received 20 January 2010; published 24 February 2010)

We have determined the bulk melting temperature T_m of nickel according to a recent interatomic interaction model via Monte Carlo simulation by two methods: extrapolation from cluster melting temperatures based on the Pavlov model (a variant of the Gibbs-Thompson model) and by calculation of the liquid and solid Gibbs free energies via thermodynamic integration. The result of the latter, which is the most reliable method, gives $T_m = 2010 \pm 35$ K, to be compared to the experimental value of 1726 K. The cluster extrapolation method, however, gives a 325° higher value of $T_m = 2335$ K. This remarkable result is shown to be due to a barrier for melting, which is associated with a nonwetting behavior.

DOI: 10.1103/PhysRevB.81.064112 PACS number(s): 64.75.−g, 64.70.D−, 82.60.Qr

I. INTRODUCTION

(Semi-)empirical interatomic interaction models for realistic atomistic simulations of reactive processes including phase transitions have become quite popular due to their superior efficiency in comparison to methods based on *ab initio* theory and their improved accuracy during the last decades. Embedded atom methods,[1–4] Stillinger and Weber type of potentials,[5–7] bond order potentials,[8–15] and tight-binding oriented potentials[16–19] are examples of models that made a significant evolution regarding their functional form and accuracy and have been parameterized for a variety of elements and mixtures. Of course, such potentials have to be thoroughly tested and compared to experimental and *ab initio* data in order to assess their performance, their weak and strong points, and their reliability in various circumstances to which they were not fitted.

An important property that one typically would like to know, and that is commonly not included in the fitting process, is the bulk melting temperature T_m according to such a model. In the present work, we have determined the melting temperature of the pure nickel component of a recent interesting semiempirical model[19] for binary systems of carbon (C) and nickel (Ni), which is based on an efficient tight-binding (TB) scheme combined with the recursion method.[20] A technologically quite relevant application possibility of this model is the study of the catalytic role of Ni in single wall carbon nanotube growth by atomistic simulation.[21–23] In this growth process the Ni droplet is sticking to the open end of the growing tube and the carbon atoms are supplied from a (hydro)carbon vapor phase via the Ni droplet to the tube. Knowledge of the bulk melting temperatures of the Ni component, which is an essential reference for the size dependent melting temperature of clusters, is of crucial importance for simulations of this process. Besides, it is an important test for the potential.

Accurate determination of T_m is not a trivial task due to the large hysteresis that typically occurs during melting and recrystallizing of a system, especially for the bulk phase. One cannot simply heat up a crystalline bulk phase in a simulation box with periodic boundary conditions and then say that T_m is equal to the temperature where the energy makes a jump and/or disorder/diffusion is observed. This can lead to quite large errors as is indeed indicated by the fact that, typically, recrystallization by cooling the liquid phase occurs at a much lower temperature. This problem has been recognized and several methods have been proposed to avoid or reduce it. One possibility is to determine T_m by extrapolation of the melting temperatures of clusters of increasing size on the basis of simple models, including Gibbs-Thompson-like models[24,25] and models which include surface melting.[26] For clusters, hysteresis is expected to be (much) smaller. However, as we will show, it can still be significant, up to an extent that it hinders an accurate determination of T_m. A second method is to construct a simulation box containing the solid and the liquid phase in contact with each other and then run simulations at various temperatures around a presumed estimate of T_m in order to find that temperature for which the phase boundary does not move.[27,28] However, even in this case, for nonrough surfaces, the results can be obscured by the presence of hysteresis, this time due to a two-dimensional (2D) nucleation barrier required for the formation of steps/islands on the solid surface.[29] From lattice Monte Carlo (MC) simulation based on the Kossel model it is well known that this 2D nucleation barrier can give rise to a large dead zone with zero growth rate in the growth rate curve.[30] However, for rough surfaces this is not the case and this method can give accurate results for T_m as has been demonstrated.[27] The third, probably the most rigorous method to determine T_m is the thermodynamic integration method[31] which allows for straightforward calculation of the free energy as a function of temperature (or pressure) for both phases. Two examples of the application of this method are given in Refs. 32 and 33. In the present paper, we have used the first and the last mentioned methods. This allowed us to assess the reliability of the cluster extrapolation method by comparing it to the more rigorous thermodynamic integration method.

In Sec. II we will give the basic ingredients of the TB model used for the total-energy evaluation in our MC simu-

lations. In Sec. III we briefly describe the standard models explaining the size dependence of the melting temperature of clusters and apply it to our simulations of the melting of Ni clusters. Section IV presents the thermodynamic integration method and the T_m resulting from it. The "discrepancy" of the latter result with that from cluster extrapolation is resolved in Sec. V. Section VI contains a brief summary and perspectives.

II. MONTE CARLO SIMULATION MODEL

Our Monte Carlo simulation model is based on an efficient TB scheme[19] in which the total energy is equal to the sum of atomic energies E_i of all atoms $i=1,\ldots N$,

$$E=\sum_{i}^{N}E_i=\sum_{i}^{N}(E_{rep,i}+E_{coh,i}). \tag{1}$$

In this expression, the repulsive atomic energy $E_{rep,i}$ is given by

$$E_{rep,i}=F\left(\sum_{j}V_R(r_{ij})\right) \tag{2}$$

where V_R is a spherical symmetric pair potential with a finite cutoff, preferentially between the first and second neighbor distances and F is a functional to optimize the transferability of the model for variable coordination environments. The cohesive atomic energy $E_{coh,i}$ in Eq. (1) is given by

$$E_{coh,i}=\int_{\infty}^{E_F}(E-\epsilon_i)n_i(E)dE=\sum_{\lambda}\int_{\infty}^{E_F}(E-\epsilon_i)n_{i\lambda}(E)dE \tag{3}$$

where $n_{i\lambda}(E)$ is the local density of states (LDOS) projected on the atomic orbital λ and $n_i(E)=\Sigma_\lambda n_{i\lambda}(E)$ is the total LDOS for atom i and where ϵ_i is the average cohesive energy per electron in a free atom. To prevent spurious charge transfer which in reality should play a minor role in C-Ni systems for which the potential has been designed,[19] a "local Fermi energy" is defined by the constraint $Z_i=\int_{\infty}^{E_F}n_i(E)dE$ where Z_i is the number of valence electrons corresponding to the basis of orbitals of atom i. The pure Ni component, used here, is described within the $3d$ basis of orbitals and $Z_i=8$.

The intrinsic computational gain of the model is based on the fact that the projected local density of states is approximated by a continued fraction expansion,

$$n_{i\lambda}(E)=-\frac{1}{\pi}\lim_{\epsilon\to 0}\cfrac{1}{z-a_1^{i\lambda}-\cfrac{b_1^{i\lambda}}{z-a_2^{i\lambda}-\cfrac{b_2^{i\lambda}}{z-a_3^{i\lambda}-b_3^{i\lambda}/(z-\ldots}}}$$

in which the $a_j^{i\lambda}$ and $b_j^{i\lambda}$ $(j=1,2\ldots)$ are directly related to the moments $\langle i\lambda|H^m|i\lambda\rangle$ $(m=1,2,\ldots)$ with H the TB Hamiltonian, and in which all higher order continued fraction coefficients $a_j^{i\lambda}$ and $b_j^{i\lambda}$ $(j=3,4\ldots)$ are taken equal to $a_2^{i\lambda}$ and $b_2^{i\lambda}$, respectively. In practice, this constant tail prolongation of the continued fraction expression implies that only the first four moments $(m=1,2,3,4)$ have to be computed, an approach which involves the neighborhood up to the second-nearest-neighbor shell. Within this approximation, the integration in Eq. (3) can be performed analytically.[34]

On top of the intrinsic gain in computational efficiency of this approach (no matrix diagonalization required), we realized a very efficient MC implementation of the method[35] by maximally employing the locality of the changes in the contributions to the moments after a MC atomic displacement and by replacing the numerical integration [Eq. (3)] by a numerically stable version of the analytical solution in Ref. 34. For pure Ni systems considered here this led to a 400 (!) times faster code, making the here presented simulations feasible.

III. MELTING OF CLUSTERS

A. Gibbs-Thompson and Pavlov

In this section we briefly present the theoretical basis of the traditional, thermodynamic models which are commonly used to explain the melting behavior of clusters. This gives us the opportunity to define the symbols for the relevant thermodynamic quantities, which are reused in subsequent sections. In these models, it is assumed that the cluster can effectively be described in a spherically symmetric geometry.

The free energy of a solid (s) or liquid (l) cluster containing N particles, $G_{P,cl}(N)$, surrounded by a more fluid phase, i.e., a liquid or vapor/vacuum (v) phase, of the same pure species can be written as

$$G_{P,cl}(N)=Ng_P+\gamma_{PP'}A_P(N) \tag{4}$$

where g_P is the bulk free energy per particle in phase P (s or l), $\gamma_{PP'}$ is the free energy per unit area of the surface between phase P and P' and $A_P(N)$ is the surface area of the cluster in phase P which is a function of N. The condition for equilibrium, i.e., $\partial G_{P,cl}/\partial N=g_{P'}$, leads (for a spherical cluster) to

$$N(g_{P'}-g_P)-\frac{2}{3}\gamma_{PP'}A_P(N)=\Delta g\rho_P V_P-\frac{2}{3}\gamma_{PP'}A_P(N)=0 \tag{5}$$

where $\Delta g=g_{P'}-g_P$, ρ_P is the (number) density and V_P is the volume of the cluster in phase P. The Gibbs free-energy difference between the bulk liquid and solid phase is equal to

$$\Delta g=\Delta h-T\Delta s\simeq\Delta h\left(1-\frac{T}{T_m}\right) \tag{6}$$

where T_m is the bulk melting temperature and where $\Delta h=h_l-h_s$ and $\Delta s=s_l-s_s$ are, respectively, the bulk enthalpy and entropy difference between the two phases. At T_m, Δh is the melting heat or latent heat and $\Delta s=\Delta h/T_m$ the melting entropy. However, whereas normally h_P and s_P have a significant dependence on temperature, the temperature dependencies of Δh and Δs are usually weak and often neglected, which justifies the most right-hand side of Eq. (6). Since the external pressure is zero in this work, which is representative for ambient conditions, enthalpy is equal to energy, i.e., $h_P=u_P$ and $\Delta h=\Delta u$. Therefore, from now on we will use en-

ergy u, with Δu being the bulk melting energy. Combining Eqs. (5) and (6) straightforwardly leads to the Gibbs-Thompson equation

$$\frac{T_{mcl}}{T_m} = 1 - \frac{2\gamma_{sl}}{\rho_s \Delta u R_s} \tag{7}$$

where T_{mcl} is the melting temperature of the cluster, and R_s is the (effective) radius of the solid cluster.

In our case of a free cluster the situation is different and we should consider the equilibrium between a solid cluster and a liquid cluster with the same number of atoms. Now the equilibrium condition is $\partial G_{l,cl}/\partial N'|_N = \partial G_{s,cl}/\partial N'|_N$. Using Eq. (4), and taking into account the density difference between liquid and solid phase, this can be worked out to

$$(g_l - g_s)N + \frac{2}{3}(\gamma_{lv}A_l - \gamma_{sv}A_s) = \Delta g \rho_s V_{s,cl} + \frac{2}{3}(q_\rho \gamma_{lv} - \gamma_{sv})A_s = 0. \tag{8}$$

where we defined $q_\rho \equiv (\rho_s/\rho_l)^{2/3}$. Then, by substitution of Eq. (6) into Eq. (8), we find the Pavlov equation,

$$\frac{T_{mcl}}{T_m} = 1 - \frac{2}{\rho_s \Delta u R_{s,cl}}(\gamma_{sv} - q_\rho \gamma_{lv}) \equiv 1 - \frac{2\Delta\gamma_{sl}}{\rho_s \Delta u R_{s,cl}} \tag{9}$$

where we defined $\Delta\gamma_{sl} \equiv \gamma_{sv} - q_\rho \gamma_{lv}$. So essentially the Pavlov equation is equal to the Gibbs-Thompson equation but with a different interpretation of the surface term, i.e., γ_{sl} is replaced by $\Delta\gamma_{sl}$. Equation (9) predicts a linear dependence of T_{mcl} on the inverse cluster radius, $1/R_s$, with T_{mcl} extrapolating to T_m at $1/R_s = 0$.

B. Results and Pavlov interpretation of cluster simulations

In Fig. 1 several heating energy curves at different "heating rates" in terms of MC cycles per degree and a cooling curve obtained from MC simulations of a free Ni cluster with 1289 atoms are presented. The initial cluster, shown in Fig. 2(a), has the Wulff shape, minimizing the surface energy at 0 K according to our interaction model and is a regular truncated octahedron. As we can see in Fig. 1 there is a large hysteresis of 470°. The fact that the energy after cooling does not reach the solid base line of the heating curve is due to the fact that the recrystallized system contains defects, as is demonstrated in Fig. 2(d). Due to the large hysteresis it can be argued that the cluster melting temperature T_{mcl} cannot be unambiguously derived from Fig. 1. For sure T_{mcl} lies within the range marked by the sharp jumps in the heating and cooling curves, but this would imply an inaccuracy of 470/2° (!) in this case. However, it is a known fact that in nature one can hardly supercool a solid, but the undercooling of a liquid phase is quite common. This is due to the fact that there is a nucleation barrier for crystallization. For melting no barrier is expected, especially for a cluster, with a permanent availability of kink sites at the edges of the surface. Using this fact implies that T_{mcl} should be taken close to the jump in the heating curve. Here we adopt a procedure that is used in calorimetric measurements and which is illustrated in Fig. 1. In this method T_{mcl} is determined by the intersection

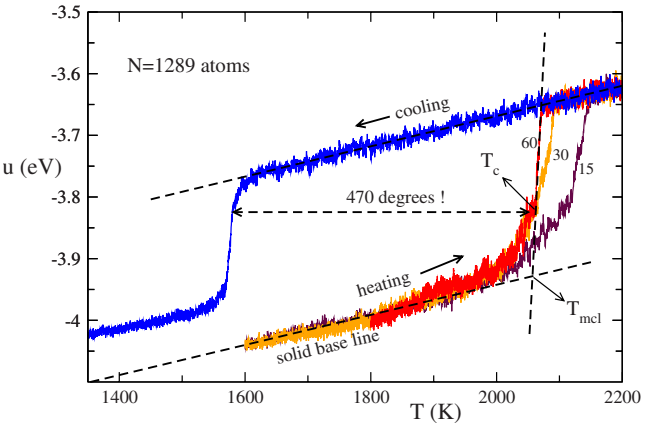

FIG. 1. (Color online) Melting energy curves for "heating rates" of 15, 30, and 60 MC cycles per degree, as indicated in the graph (one MC cycle is N MC atomic displacement trials), and a cooling energy curve for a "cooling rate" of 60 MC cycles per degree for a Ni cluster of 1289 atoms. Following the procedure in the experimental differential scanning calorimetry technique, the cluster melting temperature T_{mcl} is determined by the intersection of the solid phase base line (lower dashed line) and the vertical dashed line located at the jump in the heating curve. The energy u is in eV per particle.

of the line along the sharp jump in the heating curve and the solid base line.

Determining T_{mcl} in the described way for clusters with the number of atoms ranging from $N=38$ to $N=5635$ (see Fig. 3), and plotting T_{mcl} against $1/R_s$ leads to Fig. 4. We

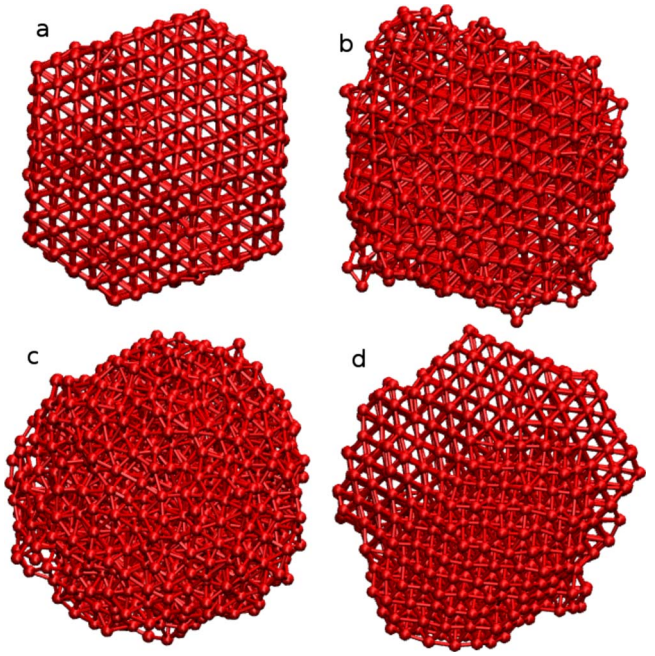

FIG. 2. (Color online) (a) Initial Wulff-shaped configuration, snapshots (b) during heating just before melting and (c) after melting, and (d) final recrystallized configuration after cooling. These configurations belong to the system and simulations with the slow "heating and cooling rates" of Fig. 1. Note that the (d) recrystallized state is not monocrystalline in this case.

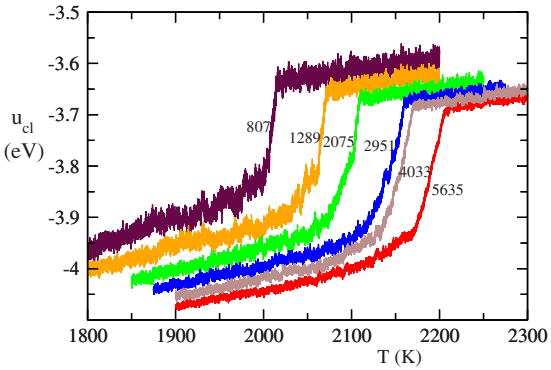

FIG. 3. (Color online) Melting energies curves for six Ni clusters. The cluster melting temperatures, T_{mcl}, which are used in Fig. 4 are determined following the procedure illustrated in Fig. 1.

have taken on purpose a systematic sequence of Wulff clusters so that the solid-vapor interfacial energy is similar for each cluster and a smooth dependence of the melting temperature on the (inverse) cluster size can be expected facilitating the extrapolation to the bulk crystal. The best straight-line fit of the cluster melting temperatures of the 6 largest clusters extrapolates, according to the Pavlov expression, to a bulk melting temperature of $T_m=2335$ K, well above the experimental value $T_{m,exp}=1726$ K.

IV. THERMODYNAMIC INTEGRATION

A. Thermodynamic integration method

The method of thermodynamic integration to determine the bulk melting temperature is based on the calculation of the Gibbs free energies as a function of temperature (or pressure) for both the liquid and the solid phases. Then, the melting temperature at a given pressure (or the equilibrium pressure at a given temperature) is given by the intersection of

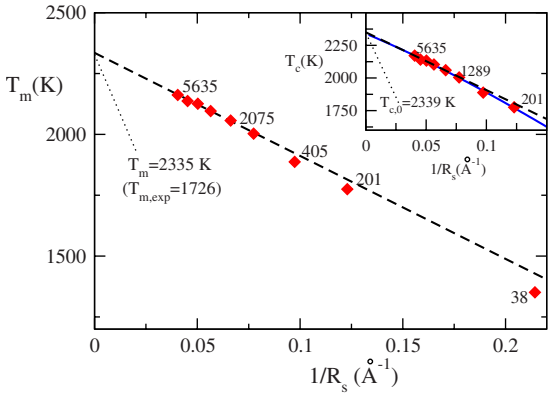

FIG. 4. (Color online) Cluster melting temperatures T_{mcl} (symbols) as a function of the inverse cluster radius, $1/R_s$. The dashed straight line is a linear fit, which extrapolates to a bulk melting temperature of 2335 K. The symbols in the inset give the temperature at which the barrier for melting vanishes, T_c (see Fig. 1) versus $1/R_s$. The dashed line in the inset is a straight-line best fit to the T_c's of largest six clusters, whereas the full line is a best fit based on Eqs. (17) and (18).

the two curves. In our case we will determine T_m at a pressure $P_0=0$.

For both liquid and solid phases the calculation based on MC simulation consists of four steps. In *step 1* the equilibrium volume, V_{eq}, at P_0 and a temperature T_0 close to a first estimate of T_m is determined by means of (NPT) MC simulation. Next, in *step 2*, the so-called λ-integration (see below) is performed to calculate the Helmholtz free energy F_P in phase $P=l,s$ from the known Helmholtz free energy of a reference system, $F_{P,ref}$, by means of (NVT) MC simulations at temperature T_0 and volume V_{eq}. Subsequently, in *step 3*, the Gibbs free energy at (P_0,T_0) is evaluated by $G_P=F_P+P_0V_{eq}$. Finally, in *step 4*, the β integration (see below) is performed to compute $G_P(P_0,T)$ as a function of T by means of (NPT) simulations at $P=P_0$ for a discrete grid of β values $(\beta=(k_BT)^{-1})$.

In the λ integration, the energy of the system is given by

$$U_P(\lambda) = (1-\lambda)U_{P,ref} + \lambda U_{P,TB} \tag{10}$$

where $U_{P,ref}$ is the energy of the reference system of known free energy and $U_{P,TB}$ is the energy according to our TB model. The Helmholtz free energy being equal to $-\beta^{-1}\ln Q(N,V_{eq},T_0)$, with $Q=\lambda_{dB}^{-3N}\int d\mathbf{r}^N \exp(-\beta U(\lambda))$ the partition function at (N,V_{eq},T_0) and λ_{dB} the de Broglie wave length, it follows that

$$\frac{dF_P}{d\lambda} = -\frac{1}{\beta}\frac{d}{d\lambda}\ln Q = \langle U_{P,TB} - U_{P,ref}\rangle_\lambda$$

$$\Rightarrow F_P = F_{P,ref} + \int_0^1 d\lambda \langle U_{P,TB} - U_{P,ref}\rangle_\lambda \tag{11}$$

For the liquid phase the reference system is a Lennard-Jones (LJ) liquid described by so-called "cut and shifted" LJ potential,

$$U_{l,LJ} = \phi(r) - \phi(r_c) = 4\epsilon\left(\left(\frac{\sigma}{r}\right)^{12} - \left(\frac{\sigma}{r}\right)^{6}\right) - \phi(r_c) \tag{12}$$

for $r<r_c$ and $U_{l,LJ}=0$ for $r\geq r_c$, where $\phi(r)$ is the standard 12-6 LJ potential and where $r_c=4\sigma$. The LJ parameters were taken equal to $\epsilon=0.21$ eV and $\sigma=2.1$ Å. These parameters were chosen such that (i) LJ liquid is supercritical to avoid phase separation, and (ii) the structure of the LJ liquid resembles that of the TB model by matching the positions of first peak in the radial distribution function, to optimize the numerical conditions of the calculation. The Helmholtz free energy $F_l(\rho,T)$ as a function of the density and T for this LJ system has been accurately parameterized in Ref. 36 and we used this parametrization.

For the solid phase, the Einstein crystal was taken as reference system, with the potential energy as a function of the atomic positions $\mathbf{r}_i$ given by

$$U_{s,Einst} = \sum_i (\alpha(\mathbf{r}_i - \mathbf{r}_{i,ref})^2 + u_0) \tag{13}$$

with α a spring constant and u_0 an irrelevant shift and where $\mathbf{r}_{i,ref}$ are the fixed positions of the Einstein reference lattice, which is a perfect fcc lattice in our case. The Einstein model

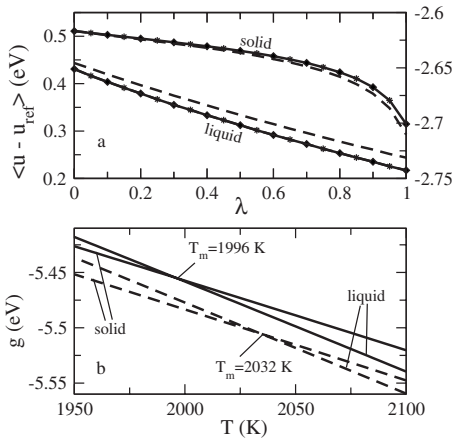

FIG. 5. (a) Simulation results for the integrand $\langle u-u_{ref}\rangle_\lambda$ in the λ integration [Eq. (11)] for the solid phase (with labels on the left vertical axis) and the liquid phase (with labels on the right vertical axis), and (b) the solid and liquid Gibbs free energies (in eV per particle) as a function of T resulting from the β integration [Eq. (15)]. The dashed and full lines are for the system with $N=256$ and $N=500$, respectively.

yields an analytical solution for the dimensionless Helmholtz free energy per particle,

$$\frac{\beta F_{s,Einst}}{N} = \beta u_0 + 3\ln(\lambda_{dB}) - \frac{3}{2}\ln\left(\frac{2\pi}{\beta\alpha}\right) - \frac{1}{N}\left[\frac{3}{2}\ln\left(N\frac{\beta\alpha}{2\pi}\right) + \ln\left(\frac{V}{N}\right)\right] \quad (14)$$

where the fourth (last) term on the right-hand side represents the finite-size correction for keeping the center of mass fixed during the simulation, necessary to avoid divergence of the Einstein reference energy for $\lambda\to 1$. V is the volume of the simulation box containing N atoms. The Einstein potential parameters were taken equal to $\alpha=12.8$ eV/Å^2, giving about the same mean-square displacement of the atoms as for the TB model, and $u_0=-5$ eV, comparable to the TB model ground-state energy of −4.44 eV per atom.

Since $P_0=0$ is our case, the Gibbs free energy at (P_0,T_0) is just $G_P(P_0,T_0)=F_P(P_0,T_0)$. Finally, using $G(\beta)=-\beta^{-1}\ln Q(N,P_0,T)$ with $Q(N,P_0,T)=\lambda_{dB}^{-3N}\int dV d\mathbf{r}^N \exp(-\beta(U+P_0V))$ the partition function at (N,P_0,T), $G_P(P_0,T)$ at any T can be computed by integrating

$$\frac{d\beta G}{d\beta} = \langle U+PV\rangle_\beta$$

$$\Rightarrow \beta G(\beta) = \beta_0 G(\beta_0) + \int_{\beta_0}^{\beta} d\beta' \langle U+P_0V\rangle_{\beta'} \quad (15)$$

where $\langle U+P_0V\rangle_{\beta'}$ is determined in (NPT) MC simulation at $P=P_0$.

B. Bulk melting temperature from thermodynamic integration

Figure 5 shows the results for the λ simulations and the Gibbs free energies as a function of T resulting from the β integrations. To investigate size effects these calculations were done for two systems of different sizes. The λ integration was performed at different temperatures T_0 for the two systems to check consistency. In all cases a cubic simulation box was used. The numbers of atoms in the two systems were $N=256$ and $N=500$, and the corresponding T_0 was taken to be equal to 2300 and 2100 K, respectively. The first $T_0=2300$ K was based on our estimate from the cluster extrapolation method. To check for hysteresis, indicating undesired phase changes, the simulations for the λ integration were first done for λ values from $\lambda=0$ to $\lambda=1$ in steps of $d\lambda=0.1$. After that, starting from the final configuration at $\lambda=1$, simulations were done for another set of λ values going back from $\lambda=0.95$ to $\lambda=0.05$, again in steps of $d\lambda=0.1$, giving a total of 21 simulation points to perform the integration in Eq. (11) based on spline interpolations between points. As we can see in Fig. 5(a), no hysteresis occurs since all points are situated on a smooth curve, both for the solid and the liquid phases. Values of the various free-energy contributions are listed in Table I for both systems. The intersection points in Fig. 5(b) give bulk melting temperatures equal to $T_{m,256}=2032\pm 45$ K, and $T_{m,500}=1996\pm 40$ K for the two systems. Although the results for the two systems are within the error margins, a difference of 36° is not very small. Although it can reasonably be expected that our result is converged, it might be interesting to perform a more detailed study of the size effects, which however is beyond the scope of the present paper. The experimental T_m being equal to 1728 K, our result for T_m can be considered as a quite reasonable performance of the TB interaction model and is considerably better than the prediction based on extrapolation in Sec. III B.

TABLE I. Values of the various free-energy contributions in the thermodynamic integration procedure where $\beta_0=(k_BT_0)^{-1}$, $F_{P,ref,0}$, and $F_{P,TB,0}$ refer to the values at T_0 and $I_\lambda=\int_0^1 d\lambda\langle U_{P,TB}-U_{P,ref}\rangle_\lambda$. Note that T_0 is different for the two system sizes (see text).

	$N=256$		$N=500$	
	Liquid	Solid	Liquid	Solid
$\beta_0F_{P,ref,0}/N$	−15.3197	−30.9277	−15.6898	−33.0325
β_0I_λ/N	−13.5784	2.2783	−14.9218	2.5276
$\beta_0F_{P,TB,0}/N$	−28.8981	−28.6494	−30.6115	−30.5049

After thoroughly checking and verifying the thermodynamic integration calculations, also by performing them with independently developed software tools for computing the free energy of the LJ liquid according to Johnson and the Einstein crystal, we consider these results much more reliable than those from cluster extrapolation as they are determined from a rigorous method without suffering from the metastability phenomena associated with the large hysteresis as observed in the cluster simulations. Hence, we conclude that T_m is about 2010 ± 35 K, which leaves us to explain the "discrepancy" with the cluster extrapolation result.

V. ANALYSIS OF CLUSTER DATA BEYOND PAVLOV, CELESTINI MODEL

In the Celestini model the cluster is not necessarily completely liquid or solid, like in the Pavlov model, but it may

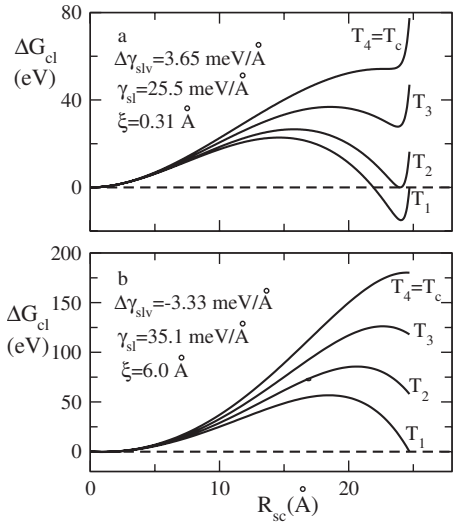

FIG. 6. The cluster Gibbs free-energy difference $\Delta G_{cl} = G_{cl}(R_{sc}) - G_{cl}(0)$ against the solid core R_{sc} for (a) positive and (b) negative spreading parameter $\Delta\gamma_{slv} = \gamma_{sv} - \gamma_{lv} - \gamma_{sl}$. The temperatures in graph (a) are $T_1 = 2081$, $T_2 = 2100$, $T_3 = 2136$, and $T_4 = T_c = 2172$ K, whereas those in graph (b) are $T_1 = 1982$, $T_2 = 2040$, $T_3 = 2100$, and $T_4 = T_c = 2162$ K.

also consist of a (spherical) solid core surrounded by a (spherical) liquid surface layer. It departs from the following expression for the Gibbs free energy of the cluster:

$$G_{cl}(R_{sc}) = g_l \rho_s V_s - \Delta g \rho_s V_{sc} + \gamma_{sl} A_{sc} + \gamma_{lv} A_{cl} + \Delta\gamma_{slv} \exp\left(\frac{R_{sc} - R_s}{\xi}\right) A_s \tag{16}$$

where γ_{sl} is the solid-liquid surface free energy and $\Delta\gamma_{slv}$ is the so-called spreading parameter defined as $\Delta\gamma_{slv} \equiv \gamma_{sv} - \gamma_{lv} - \gamma_{sl}$. V_{cl} and V_{sc} are the spherical volumes of the total cluster and the solid core with radii R_{cl} and R_{sc} and surface areas A_{cl} and A_{sc}, respectively, and ξ is a length representing the decay distance of the interaction between the *sl* and the *lv* surfaces. A_s and V_s are the surface area and volume of a completely solid cluster as before, with $\rho_s V_s = \rho_l V_l = N$. It has been shown that Eq. (16) with positive $\Delta\gamma_{slv}$ can describe surface melting. This is illustrated in Fig. 6(a) where we plotted $G_{cl}(R_{sc}) - G_{cl}(0)$ against R_{sc} for a large Ni cluster with 5635 atoms at different temperatures $T_i (i = 1, \ldots 4)$, using values for γ_{sl} and ξ which are derived from a fit of the model to the simulation data (see below). For $T = T_1$, $G_{cl}(R_{sc} = R_s) = G_{cl}(0)$; i.e., the completely liquid cluster and the completely solid cluster are equally stable. However, G_{cl} has a minimum at a solid core radius $R_{sc} < R_s$, which implies surface melting. For the $T = T_2$, the free energy of this coexistence state with a solid core and a liquid layer becomes equal to that of the completely liquid cluster. For $T_2 < T < T_4$, the completely liquid cluster would be the most stable state but there is an energy barrier for melting. This barrier vanishes at T_4, which we will call T_c. At T_c, $dG_{cl}/dR_{sc} = d^2G_{cl}/d^2R_{sc} = 0$ and these conditions can be worked out to

$$\frac{T_c}{T_m} = 1 - \frac{2\gamma_{sl}}{\rho_s \Delta u R_{sc}} \frac{(1 - \xi/R_{sc})}{(1 - 2\xi/R_{sc})} \tag{17}$$

as has been presented by Celestini *et al.* Since we have two conditions, i.e., $dG_{cl}/dR_{sc} = 0$ and $d^2G_{cl}/d^2R_{sc} = 0$, a second equation can be derived for R_{sc}, which for $\xi \ll R_{sc}$ can be approximated by

$$R_{sc} \simeq R_s + \xi \ln\left(\frac{2\gamma_{sl}\xi^2}{\Delta\gamma R_s^2}\right). \tag{18}$$

If we substitute Eq. (18) into Eq. (17), we obtain T_c as a function of $1/R_s$, allowing for a straightforward fit to obtain values for T_m, γ_{sl}, $\Delta\gamma$, and ξ. Since γ_{sl} is normally positive, Eq. (17) tells us that T_c should be below T_m for any cluster size. Therefore, if we rely on the $T_m = 2010$ K from the thermodynamic integration method, Eq. (17) can never explain our results. From a best fit of Eq. (17), after substitution of Eq. (18), to the T_c's of all clusters except the smallest with $N = 38$ atoms, shown in the inset of Fig. 4, we find $T_m = 2339$ K, $\gamma_{sl} = 25.5$ meV/Å, $\Delta\gamma = 3.25$ meV/Å, and $\xi = 0.31$ Å, which were used for Fig. 6(a). So the predicted T_m from this model is close to that predicted by the Pavlov model in this case. However, since the number of parameters is rather high with respect to the available simulation data, the accuracy of γ_{sl} and especially $\Delta\gamma$, estimated on the basis of just the fitting process, is not very high, with errors of about 20% and 40%, respectively. Instead, the error for T_m is much smaller in the sense that the range of T_m values allowing for a reasonable fit according to this model and positive $\Delta\gamma$ is restricted to $2330 < T_m < 2350$ K.

In the usually not considered case that $\Delta\gamma_{slv} < 0$ the situation becomes different. This is illustrated in Fig. 6(b). For the surface parameters indicated in the figure, at $T_1 = 1982$, below T_m, the free energy of a completely liquid cluster is equal to that of a completely solid cluster. However, there is a large barrier for melting and there is no minimum at some $R_{sc} < R_s$, which means that surface melting is energetically not favorable due to a large γ_{sl} and/or a small $\gamma_{sv} - \gamma_{lv}$. For the other temperatures, all well above $T_m = 2010$ K, the completely liquid cluster is more stable, but there is a significant barrier for melting. Finally, at $T_4 = T_c = 2162$ K, 150° (!) above T_m, this barrier vanishes. Now the condition at T_c is $dG_{cl}/dR_{sc}|_{R_{cl}=R_s}$ which leads to

$$\frac{T_c}{T_m} = 1 - \frac{\Delta\gamma_{slv}}{\rho_s \Delta u \xi} - \frac{2\gamma_{sl}}{\rho_s \Delta u R_s}. \tag{19}$$

This equation predicts a linear dependence of T_c on $1/R_s$, similar to what the Pavlov equation does for T_{mcl}. However, in the large cluster limit T_c does not converge to T_m, but to a higher temperature $T_m - \Delta\gamma_{slv} T_m/(\rho_s \Delta u \xi)$. This behavior is fully consistent with our simulations results for T_c versus $1/R_s$, shown in the inset of Fig. 4, where T_c has been determined as indicated in Fig. 1. In fact, from the inset of Fig. 4 and with ξ taken equal to 6 Å, the surface parameters $\gamma_{sl} = 35.1$ meV/Å^2 and $\Delta\gamma_{slv} = -3.33$ meV/Å^2 used in Fig. 6(b), are obtained by the slope and the intersection with the vertical axis at $1/R_s = 0$, respectively, of a best linear fit through the temperatures T_c. Thus, the Celestini model, but

with a negative $\Delta\gamma_{slv}$, can describe a cluster melting process without surface melting, i.e., a nonwetting behavior. In that case the melting can be retarded by a significant barrier, which for the larger clusters lead to melting temperatures well above T_m. In fact, in snapshot b of Fig. 2, taken at a temperature just before complete melting, the nonwetting behavior is confirmed by the fact that large parts of the surface are still ordered, and that some surface melting only takes place at the corners of the solid cluster, which can explain the change in the slope in the energy curves before melting. We also note that a decay length of 6 Å for the interaction between the *sl* and the *lv* surfaces seems much more realistic than the value $\xi=0.31$ Å that followed from the best fit of Eq. (17) to the simulation data.

To some extent, one can argue that the observed retardation of melting is a matter of time scale of the simulation. However, we slowed down the "heating rate" until the melting temperature did not change anymore (see Fig. 1). Thus, in practice, this problem is difficult to control and undermines the reliability of the determination of T_m by extrapolation from the cluster melting temperatures. Note that this is also true for the case that $\Delta\gamma_{slv}>0$ with surface melting. Indeed, looking at Fig. 6(a), the melting of the cluster could occur at any temperature between T_2 and T_c. In addition, from the cluster melting data alone, i.e., without knowing T_m or having information about surface melting, it cannot even be decided whether $\Delta\gamma_{slv}$ is positive or negative.

It is interesting to compare our values for γ_{sl} with those from the Turnbull expression[37,38]

$$\gamma_{sl}=C_T L\rho_s^{2/3} \tag{20}$$

where $L\simeq\Delta u$ is the latent heat per atom and C_T is the so-called Turnbull coefficient, which was originally estimated to be equal to $C_T=0.45$ for metals. Recent efforts based on atomistic simulation[39–41] have roughly confirmed the validity of the Turnbull expression, but with somewhat larger values for C_T between 0.47 and 0.6 (Ref. 42) for an fcc crystal. In our case this corresponds to $33.3<\gamma_{sl}<42.6$ meV/Å^2, a range which is consistent with the value based on Eq. (19) and larger than that from Eq. (17).

The nonwetting behavior we find is contrary to previous results for Ni cluster melting,[43] based on a bond order type of potential.[44,45] So the disagreement may come from the difference in the interaction potentials. For our TB model we can say that it reproduces reasonably well the surface energies of several flat *sv* surfaces.[19] On the other hand, the disagreement may also be due to the fact that we started from Wulff clusters, minimizing γ_{sv} and consequently $\Delta\gamma_{slv}$. It is indeed more likely for a Wulff cluster to have a negative spreading parameter than for less stable clusters.

To conclude, we now give an extension of the Celestini model which includes the difference in density between liquid and solid phase. For a not too large density difference, the cluster surface A_{cl} as a function of the solid core radius R_{sc} is very well approximated by

$$A_{cl}(R_{sc})=q_\rho A_s+(1-q_\rho)\frac{R_{sc}}{R_s}A_{sc} \tag{21}$$

where $q_\rho=(\rho_s/\rho_l)^{2/3}$ as before. Equation (21) yields $A_{cl}(R_{sc}=R_s)=A_s$, $A_{cl}(R_{sc}=0)=q_\rho A_s=A_l$, and $A_{cl}=A_s$ for any R_{sc} if $\rho_s=\rho_l$, as it should be. Substitution of Eq. (21) into Eq. (16) leads to

$$G_{cl}(R_{sc})=g_l\rho_s V_s-\Delta g\rho_s V_{sc}+\left((1-q_\rho)\frac{R_{sc}}{R_s}\gamma_{lv}+\gamma_{sl}\right)A_{sc}+q_\rho\gamma_{lv}A_s+\Delta\gamma_{slv}\exp\left(\frac{R_{sc}-R_s}{\xi}\right)A_s \tag{22}$$

For $R_{sc}=R_s$ and $R_{sc}=0$ (with a vanishing exponential term for $R_{sc}=0$), Eq. (22) is consistent with Eq. (4). With Eq. (22) and negative spreading parameter $\Delta\gamma_{slv}$, the condition $dG_{cl}/dR_{sc}|_{R_{cl}=R_s}=0$ at T_c now leads to

$$\frac{T_c}{T_m}=1-\frac{\Delta\gamma_{slv}}{\rho_s\Delta u\xi}-\frac{2\gamma_{sl}+3(1-q_\rho)\gamma_{lv}}{\rho_s\Delta u R_s} \tag{23}$$

which gives back Eq. (19) for $q_\rho=1$. According to Eq. (23), the straight-line analysis shown in the inset of Fig. 4 still make sense, but the extraction of γ_{sl} from the slope is much more difficult since γ_{lv} and also q_ρ for a cluster are not (accurately) known. However, since $q_\rho>1$ and $\gamma_{lv}>0$, the induced correction for γ_{sl} is positive.

Finally, for the wetting case, i.e., for positive $\Delta\gamma_{slv}$, the expression for T_c/T_m including the density difference, deduced by imposing $dG_{cl}/dR_{sc}=d^2G_{cl}/d^2R_{sc}=0$ with G_{cl} from Eq. (22), becomes

$$\frac{T_c}{T_m}=1-\frac{2\gamma_{sl}}{\rho_s\Delta u R_{sc}}\frac{(R_{sc}-\xi)}{(R_{sc}-2\xi)}-\frac{3(1-q_\rho)\gamma_{lv}}{\rho_s\Delta u R_s}. \tag{24}$$

In the limit of large clusters both correction terms at the right-hand side vanish, so that $T_c\to T_m$ in this limit. As in the nonwetting case, the correction of γ_{sl} due to the last term on the right-hand side of Eq. (24) will be positive.

VI. SUMMARY, PERSPECTIVES

We have determined the bulk melting temperature T_m of the pure Nickel component of a recent semiempirical interatomic interaction model,[19] based on a TB framework, for binary C-Ni systems via MC simulation. Rigorous calculation of the Gibbs free energies for the liquid and solid phases by using the thermodynamic integration method leads to $T_m=2010\pm35$ K, not too far from the experimental melting temperature $T_{m,exp}=1726$ K.

We also performed simulations of the melting of a sequence of Wulff clusters, with sizes ranging from $N=38$ to

$N=5635$ atoms. Plotting the observed cluster melting temperatures against the inverse cluster radius gives approximately a straight line, but extrapolation of this line according to the Pavlov equation suggests a T_m equal to 2335 K, 325° higher than the T_m from thermodynamic integration. We found an explanation for the observed "discrepancy" by analyzing our cluster data in terms of the Celestini model. However, contrary to the usual case, for which the Celestini model gives an appropriate correction to the Pavlov model due to the effect of surface melting, our data require a negative value for the spreading parameter $\Delta\gamma=\gamma_{sv}-\gamma_{lv}-\gamma_{sl}$, implying a nonwetting behavior, i.e., no surface melting occurs, or at least it does not occur at the usual relatively low temperatures as predicted when $\Delta\gamma$ is positive. We have shown by Eq. (19) [or Eq. (23)] that for negative $\Delta\gamma$ the cluster melting temperature against the inverse radius follows a straight line, which, however, does not extrapolate to T_m in the large cluster limit but to a higher temperature. This can explain our observation of cluster melting temperatures lying above T_m for the large clusters due to a barrier for melting which only vanishes at a $T_c > T_m$.

Usually, in literature, the T_m resulting from cluster extrapolation is not compared with that from the more rigorous thermodynamic integration method, the latter method being more complicated and laborious. Here we have shown that a straight line of the observed cluster melting temperature against the inverse cluster radius is no guarantee for a good approximation of T_m via extrapolation.

Since our finding is remarkable, one should be careful with definitive conclusions. Theoretically it could be possible that the Johnson expression and/or parametrization[36] for the LJ liquid is so inaccurate, contrary to what is claimed and what in commonly believed, that it can give rise to an error in T_m of more than 300 K. It would be very useful to have an independent confirmation of our results, for example, by an alternative and accurate determination of the effective surface-free energies γ_{sv} and γ_{lv}, which should be enough to enable such confirmation. While it seems that γ_{sl} can be determined rather accurately nowadays using recent simulation techniques,[39–41,46,47] it is not so clear to which extent these techniques and/or results can be used for or extrapolated to *sv* and especially *lv* surfaces. It would be very useful to find an answer to these questions and, if necessary, to develop additional techniques for the determination of γ_{sv} and γ_{lv}.

ACKNOWLEDGMENT

We wish to thank PAN-H ANR (Mathysse) for support.

[1] M. W. Finnis and J. E. Sinclair, Philos. Mag. A **50**, 45 (1984).
[2] M. I. Baskes, Phys. Rev. Lett. **59**, 2666 (1987).
[3] M. I. Baskes, J. S. Nelson, and A. F. Wright, Phys. Rev. B **40**, 6085 (1989).
[4] J. Cai and J.-S. Wang, Phys. Rev. B **64**, 035402 (2001).
[5] F. H. Stillinger and T. A. Weber, Phys. Rev. B **31**, 5262 (1985).
[6] J. F. Justo, M. Z. Bazant, E. Kaxiras, V. V. Bulatov, and S. Yip, Phys. Rev. B **58**, 2539 (1998).
[7] N. A. Marks, Phys. Rev. B **63**, 035401 (2000).
[8] J. Tersoff, Phys. Rev. Lett. **56**, 632 (1986).
[9] J. Tersoff, Phys. Rev. B **38**, 9902 (1988).
[10] D. W. Brenner, Phys. Rev. B **42**, 9458 (1990).
[11] D. W. Brenner, O. A. Shenderova, J. A. Harrison, S. J. Stuart, B. Ni, and S. B. Sinnott, J. Phys.: Condens. Matter **14**, 783 (2002).
[12] A. C. T. van Duin, S. Dasgupta, F. Lorant, and W. A. Goddard III, J. Phys. Chem. A **105**, 9396 (2001).
[13] A. C. T. van Duin, A. Strachan, S. Stewman, Q. Zhang, X. Xu, and W. A. Goddard III, J. Phys. Chem. A **107**, 3803 (2003).
[14] J. H. Los and A. Fasolino, Phys. Rev. B **68**, 024107 (2003).
[15] J. H. Los, L. M. Ghiringhelli, E. J. Meijer, and A. Fasolino, Phys. Rev. B **72**, 214102 (2005).
[16] D. G. Pettifor, Phys. Rev. Lett. **63**, 2480 (1989).
[17] D. G. Pettifor and I. I. Oleinik, Phys. Rev. B **59**, 8487 (1999).
[18] I. I. Oleinik and D. G. Pettifor, Phys. Rev. B **59**, 8500 (1999).
[19] H. Amara, J. M. Roussel, C. Bichara, J. P. Gaspard, and F. Ducastelle, Phys. Rev. B **79**, 014109 (2009).
[20] R. Haydock, V. Heine, and M. J. Kelly, J. Phys. C **5**, 2845 (1972).
[21] C. Journet, W. K. Maser, P. Bernier, A. Loiseau, M. Lamy de la Chapelle, S. Lefrant, P. Deniard, R. Lee, and J. E. Fischer, Nature (London) **388**, 756 (1997).
[22] J. Gavillet, A. Loiseau, C. Journet, F. Willaime, F. Ducastelle, and J.-C. Charlier, Phys. Rev. Lett. **87**, 275504 (2001).
[23] J. Gavillet, J. Thibault, O. Stephan, H. Amara, A. Loiseau, C. Bichara, J.-P. Gaspard, and F. Ducastelle, J. Nanosci. Nanotechnol. **4**, 346 (2004).
[24] P. Buffat and J. P. Borel, Phys. Rev. A **13**, 2287 (1976).
[25] P. Pavlov, Z. Phys. Chem., Stoechiom. Verwandtschaftsl. **65**, 1 (1909); **65**, 545 (1909).
[26] F. Celestini, R. J.-M. Pellenq, P. Bordarier, and B. Rousseau, Z. Phys. D: At., Mol. Clusters **37**, 49 (1996).
[27] J. R. Morris and X. Song, J. Chem. Phys. **116**, 9352 (2002).
[28] For a review of the method, see F. D. Di Tolla, E. Tosatti, and F. Ercolessi, in *Monte Carlo and Molecular Dynamics of Condensed Matter Systems*, Conference Proceedings, edited by K. Binder and G. Ciccotti (SIF, Bologna, 1996), Vol. 49, Chap. 14, p. 346.
[29] W. K. Burton, N. Cabrera, and F. C. Frank, Philos. Trans. R. Soc. London, Ser. A **243**, 299 (1951).
[30] G. H. Gilmer and P. Bennema, J. Cryst. Growth **13-14**, 148 (1972).
[31] A review of the method is given in: D. Frenkel and B. Smit, *Understanding Molecular Simulation* (Academic Press, San Diego, CA, 2002).
[32] E. J. Meijer and D. Frenkel, J. Chem. Phys. **94**, 2269 (1991).
[33] L. M. Ghiringhelli, J. H. Los, E. J. Meijer, A. Fasolino, and D. Frenkel, Phys. Rev. Lett. **94**, 145701 (2005).
[34] G. Allan, M. C. Desjonqueres, and D. Spanjaard, Solid State Commun. **50**, 401 (1984).
[35] J. H. Los, C. Bichara, and R. J. M. Pellenq (unpublished).

[36] J. K. Johnson, J. A. Zollweg, and K. E. Gubbins, Mol. Phys. **78**, 591 (1993).
[37] D. Turnbull, J. Appl. Phys. **21**, 1022 (1950).
[38] D. Turnbull and R. E. Cech, J. Appl. Phys. **21**, 804 (1950).
[39] R. L. Davidchack and B. B. Laird, Phys. Rev. Lett. **85**, 4751 (2000).
[40] J. J. Hoyt, M. Asta, and A. Karma, Phys. Rev. Lett. **86**, 5530 (2001).
[41] J. R. Morris, Phys. Rev. B **66**, 144104 (2002).
[42] R. L. Davidchack and B. B. Laird, Phys. Rev. Lett. **94**, 086102 (2005).
[43] E. J. Neyts and A. Bogaerts, J. Phys. Chem. C **113**, 2771 (2009).
[44] Y. Yamaguchi and S. Maruyama, Eur. Phys. J. D **9**, 385 (1999).
[45] Y. Shibuta and S. Maruyama, Chem. Phys. Lett. **437**, 218 (2007).
[46] Q. Jiang and F. G. Shi, Mater. Lett. **37**, 79 (1998).
[47] M. Attarian Shandiz and A. Safaei, Mater. Lett. **62**, 3954 (2008).